Advanced Fiber Materials (2023) 5:1905–1918
https://doi.org/10.1007/s42765-023-00313-4

RESEARCH ARTICLE

Developing Thick Cardiac Tissue with a Multilayer Fiber Sheet for Treating Myocardial Infarction

Junjun Li[1,2] · Xiang Qu[1,2] · Li Liu[1,2] · Lingjun Li[1] · Ying Hua[1] · Jingbo Zhang[1] · Masako Ishida[1] · Noriko Yoshida[2] · Akiko Tabata[1] · Nagako Sougawa[1,3] · Emiko Ito[1] · Noriko Mochizuki-Oda[1] · Akima Harada[1] · Takuji Kawamura[1] · Ryohei Matsuura[1] · Yingzhe Wang[4] · Keisuke Morishima[4,5] · Shigeru Miyagawa[1] · Yoshiki Sawa[1,6]

Received: 27 March 2023 / Accepted: 25 June 2023 / Published online: 31 July 2023

Abstract

Human-induced pluripotent stem cell (hiPSC)-derived cardiac patches have been extensively used for treating myocardial infarction and have shown potential for clinical application. However, the limited patch thickness can hamper its therapeutic effect. We previously developed a fibrous scaffold that allowed the formation of well-organized cardiac tissue constructs. In the present study, based on the above technology, we developed a three-dimensional multilayer fibrous scaffold with dynamic perfusion, on which approximately 20 million hiPSC-derived cardiomyocytes (CMs) could be seeded in a single step and organized into 1 mm thick and viable tissue. The multilayer cardiac tissue demonstrated enhanced contractile properties and upregulated cytokine secretion compared with the control group. Notably, when used on the myocardial infarction model, the multilayer group showed improved functional recovery and less fibrosis. These results indicated that the appropriate hiPSC-CM dose requires careful evaluation in developing clinical therapy. The multilayer cardiac tissue group demonstrated significant improvement than the control group, indicating that higher doses of transplanted cells may have improved therapeutic effects in treating myocardial infarction.

Keywords Fiber · Tissue engineering · Pluripotent stem cell · Cardiomyocyte · Myocardial infarction · Regenerative therapy

Junjun Li and Xiang Qu have contributed equally to this work.

✉ Li Liu
li-liu@surg1.med.osaka-u.ac.jp

✉ Shigeru Miyagawa
miya-p@surg1.med.osaka-u.ac.jp

✉ Yoshiki Sawa
sawasec@sahs.med.osaka-u.ac.jp

[1] Department of Cardiovascular Surgery, Osaka University Graduate School of Medicine, 2-2 Yamadaoka, Suita 565-0871, Japan

[2] Frontier of regenerative medicine, Osaka University Graduate School of Medicine, 2-2 Yamadaoka, Suita 565-0871, Japan

[3] Department of Physiology, Osaka Dental University, 8-1 Kuzuha Hanazono-cho, Hirakata 573-1121, Japan

[4] Department of Mechanical Engineering, Graduate School of Engineering, Osaka University, Suita 565-0871, Japan

[5] Global Center for Medical Engineering and Informatics, Osaka University, Osaka 565-0071, Japan

[6] Division of Health Sciences, Osaka University Graduate School of Medicine, Suita 565-0871, Japan

Introduction

Human-induced pluripotent stem cells (hiPSC)-derived cardiomyocytes (CMs) have demonstrated outstanding potential in treating heart failure. Several pluripotent stem cell-based therapies have entered clinical trial phases [1]. These therapies mainly use two intensively evaluated [2–7] delivery methods: intramyocardial injection and epicardial patches. Injections efficiently deliver cells to the infarcted myocardium with long-term cell retention and functional recovery [8–10]. However, this method requires many cells because of the low retention ratio, and post-transplantation arrhythmia [10, 11] may hamper its potential clinical application. Consequently, many groups are working on patch-based therapy [12–17]. Patch-based approaches are safe and effective and can provide a structure for strengthening the infarcted ventricle [18], which operates under high pressure and with increased blood flow. Additionally, the hiPSC-CM patch may promote angiogenesis and enhance heart function recovery, both mediated by the cytokine-paracrine effect

[19]. To date, no arrhythmia events in myocardial infarction (MI) models have been reported after cardiac patch transplantation. Moreover, in our group, the first clinical trial of hiPSC-CM sheet transplantation was performed in patients with severe ischemic cardiomyopathy, and the therapeutic effect was confirmed with no tumorigenesis [19, 20]. However, the effectiveness of stem cell therapy relies more on cytokine than on remuscularization [21–23].

The critical issue for good remuscularization in infarcted myocardium is the preparation and transplantation of thick and viable tissue grafts. The overlay approaches have been used to create thick tissues [24–28]. Cardiac tissue with a thickness > 600 μm [26] was prepared and used on the rat MI model. This approach requires the preparation and overlaying of single-layer cell sheets, which may be labor-intensive and costly. We have previously created a cardiac tissue with a thickness of 160 μm by simple one-step plating of hiPSC-CMs on a thin layer of biodegradable fiber. The cardiac tissue showed the capability to repair MI in a rat model [12]. The graft showed enhanced angiogenesis between the host and graft by fabricating the fiber scaffold loaded with pro-angiogenesis factor [29]. Furthermore, a large-size fiber scaffold was used to create an up-scaled hiPSC-CM patch for treating MI in a mini pig model [30]. Here, we prepared multilayer fibers to create thicker cardiac tissue using a one-step seeding process. Since perfusion is vital for the survival of engineered tissue [31, 32], enhanced perfusion devices were used to promote the supply of nutrients and oxygen to the tissue. The multilayer tissue was cultured on an oblique holder to reduce the shear stress damage by the dynamic flow. After five days of dynamic culture, the multilayer tissue demonstrated enhanced contractile properties and upregulated cytokine secretion compared with the control group. When used for transplantation, the multilayer group showed improved ejection fraction and less fibrosis.

Methods

Preparation of Human iPSCs and Differentiation of CMs

The HLA-homo hiPSC line for clinical research (Ff-l01, CiRA, Japan) was maintained and differentiated as previously reported [12]. All experiments were performed following the Osaka University guidelines. After one month of differentiation, CM colonies were collected and dissociated into single cells by stirring for 1–2 h at 37 °C in a protease solution: 0.1% collagenase type I, 0.25% trypsin, 1 U/mL DNase I, 116 mM NaCl, 20 mM hydroxyethylpiperazine ethane sulfonic acid, 12.5 mM NaH_2PO_4, 5.6 mM glucose, 5.4 mM KCl, and 0.8 mM $MgSO_4$ (pH 7.35). The CM purity was characterized using flow cytometry, and high-purity CMs (> 85%) were used for subsequent experiments.

Flow Cytometry

The hiPSC-CMs were dissociated, fixed with 4% paraformaldehyde for 10 min, and incubated with anti-TnT2 antibodies (1:200; sc-20025, Santa Cruz Biotechnology) or isotype-matched antibodies (BD Phosphoflow: 557,782) for 8 h at 4 °C. The cells were then washed with Dulbecco's phosphate-buffered saline (PBS) once and incubated with Alexa Fluor 488 anti-mouse IgG (1:1,000; A11029; Thermo Fisher). Flow cytometry was performed using a fluorescence-activated cell sorting Canto II flow cytometer (BD Biosciences, USA), and the data were analyzed using the FlowJo software (Treestar Inc., USA).

Fabrication of Multilayer Fiber Scaffold

Poly (D,L-lactic-co-glycolic acid) (PLGA, 75/25, Sigma, USA) was mixed with hexafluoro-2-propanol (Wako, Japan) at 20% (w/w). PLGA fibers were fabricated by electrospinning at 20 kV using a commercial machine (NF-103, MECC, Japan). The solution was loaded into a 5-mL syringe with an attached needle (0.7 mm). A grounded rotating drum was used at 700 rpm to collect aligned fibers (AFs). AFs were prepared with different spin times: 30 min for high-density AFs (H-AFs) and 10 min for low-density AFs (L-AFs). The distance between the tip and collector was maintained at 120 mm. Before spinning, a layer of aluminum foil was attached to the drum for the fiber transfer procedure. AFs were collected on the aluminum foil and peeled off using a Scotch tape (Scotch™, 3 M, US) frame (external size: 1.5×1.5 cm^2; inner size: 1×1 cm^2). Scotch tape frames with one layer of H-AFs and four L-AFs were bonded to form the multilayer (MLA) fiber scaffold (Fig. S1). The control group contained only one layer of H-AF. A thicker multilayer fiber sheet was fabricated by adding another four top-layer fiber sheets above the bottom-layer fiber sheet, with a spacing of 150 μm between the two layers.

Multilayer Tissue Preparation

The cells were filtered with a 40-μm strainer (BD Falcon, USA) and resuspended at different concentrations (single-layer fiber sheet: 0.5×10^7 cells; multilayer fiber sheets: 1, 2, and 4×10^7 cells) in serum-supplemented medium: 40% high glucose Dulbecco's modified Eagle's medium (Sigma-Aldrich), 40% Iscove's modified Dulbecco's medium (Sigma-Aldrich), 20% fetal bovine serum (Gibco, USA), 1% minimum essential medium non-essential amino

acid solution (Sigma-Aldrich), and 0.1% penicillin-streptomycin (Gibco), and 0.5% L-glutamine (Sigma-Aldrich). In addition, a 10-μM Rho-kinase inhibitor (Wako) was added to improve cell survival. The cell suspension (300 μL) was plated onto a multilayer fiber sheet. After 1 h, 1 mL of the medium was gently added to the dish. After another 3 h, the fiber sheet was gently inserted into the polydimethylsiloxane holder, and 30 mL of medium was added to the dish. The tissue was incubated for one day without stirring to avoid disturbance. The magnetic stirrer was run at 250 rpm the next day. The tissue was cultured for five days before subsequent analysis.

In vivo Transplantation

Animal experiments were approved by the ethics committee of Osaka University and performed following the committee's guidelines. To create an MI model, seven-week-old male F344/NJcl-rnu/rnu rats (CLEA Japan, Tokyo, Japan) were anesthetized using isoflurane inhalation (1.5%; Mylan Inc., Tokyo, Japan). After intubation and mechanical ventilation, a thoracotomy was performed between the fourth and fifth intercostal spaces. MI was induced by ligation of the left coronary artery, as described previously [33, 34]. The cardiac tissue was cultured for one day in vitro before being used for transplantation. Four groups of samples were used for transplantation: MLA, control (single-layer fiber with 5×10^6 cells), vehicle (with ligation but without treatment), and sham (open-chest operation without ligation) groups. The tissue was pre-treated with laminin (iMatrix-511) solution (1:100) in 20% serum-supplemented medium at 25 °C for 5 min. Then the frame was cut, and the cardiac tissue was placed on the epicardium and covered with Beriplast P (CSL Behring, USA). Echocardiography was performed using an ultrasound machine (Philips SONOS 7500; Amsterdam, Netherlands) with an annular array transducer operating at 12 Mhz. Left ventricular (LV) ejection fraction (LVEF) was calculated using the Eqs. (1) and (2):

$$LVEDV(ml) = \frac{7}{2.4 + Dd} * Dd^3 \quad (1)$$

$$LVESV(ml) = \frac{7}{2.4 + Ds} * Ds^3 \quad (2)$$

Rats with and without MI were sacrificed four weeks post-surgery, and the hearts were harvested and used to prepare 7-μm-thick cryosections for histology and immunostaining. The root mean square of successive differences (RMSSD) was introduced to represent heart rate variability(HRV). The R-R interval of consecutive heartbeats was measured using echocardiography data.

Histology

The hiPSC-derived cardiac tissues were washed three times with PBS and fixed in formaldehyde for paraffin sectioning. Thin sections (8 μm) were cut and stained with hematoxylin and eosin (HE) (Muto Chemical Corporation, Japan). The degree of fibrosis was determined using Picrosirius red staining. The fibrotic area was calculated as the ratio of the total interstitial fibrosis area to the total LV area of an LV section using MetaMorph software (Molecular Devices, Sunnyvale, CA, USA). Inflammatory reactions were assessed using immunohistochemistry for CD68 (mouse monoclonal IgG, 1:100; Abcam: 955). The sections were observed under a CKX41 microscope (Olympus) or BIOREVO fluorescence microscope (KEYENCE Corporation). The positivity of CD68 was calculated using the ImageJ software (NIH, USA).

Simulation

The fluid flow velocity and shear stress distribution around the MLA tissue were simulated using the COMSOL software (COMSOL Multiphysics). The cardiac tissue size was set to 1×1×1 mm and placed at a 30° inclination. Multiple flow rates were used to analyze the corresponding flow velocity and shear stress distribution around the tissue.

Immunostaining and Imaging

Tissues were fixed in 4% paraformaldehyde for 0.5 h, permeabilized with 0.5% (v/v) Triton X-100 in Dulbecco's PBS (D-PBS) for 1 h, and immersed in blocking solution at 4 °C for 16 h. The tissues were then incubated with the primary antibodies: anti-α-actinin (1:1,000; A7811; Sigma-Aldrich), anti-troponin T2 (TnT2; 1:200; SC-20025; Santa Cruz Biotechnology, Dallas, TX, USA), anti-connexin 43 (Cx43; 1:200; C6219; Sigma-Aldrich), anti-collagen I (1:200; C2456; Sigma-Aldrich), anti-collagen III (1:200; ab7778; Abcam), and anti-fibronectin (1:200; ab2413; Abcam) at 4 °C overnight. The tissues were then rinsed with PBS and incubated with the secondary antibodies: Alexa Fluor 594 anti-mouse IgG (715-586-150; Jackson ImmunoResearch, West Grove, PA, USA), DyLight-594 anti-mouse IgM (715-516-020; Jackson ImmunoResearch), Alexa Fluor 647 anti-rabbit IgG (A21245; Thermo Fisher), Alexa Fluor 546 anti-rabbit IgG (A10040; Thermo Fisher), and Alexa Fluor 488 anti-rabbit IgG (A21202; Thermo Fisher) at a dilution of 1:300 in blocking buffer at 25 °C for 1 h. The stain 4′,6-diamidino-2-phenylindole (DAPI) (300 nM; Wako Pure Chemical Industries, Ltd.) was used to stain the nuclei

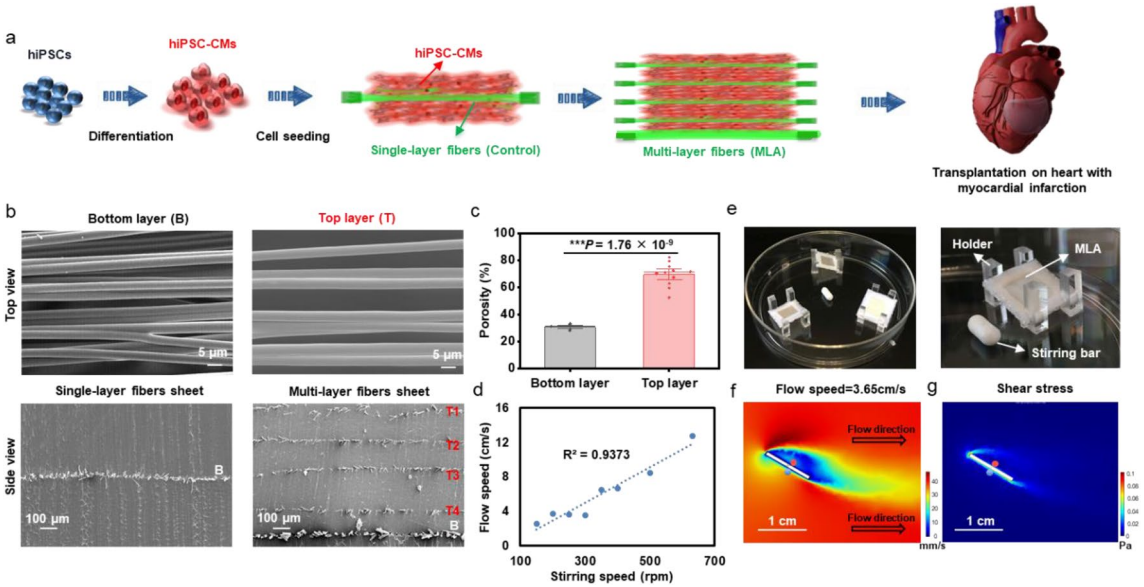

Fig. 1 Aligned multilayer fiber sheets. **a** Schematics of construction and transplantation of cardiac tissue with multilayer fiber sheet. **b** Representative scanning electron microscope images of bottom and top-layer fibers from single-layer and multilayer sheets' top and side views. **c** Scaffold porosity of bottom and top-layer fiber sheets. Data are represented as means ± SEM, Bottom: $n = 7$ sheets; Top: $n = 11$ sheets. ***$P < 0.001$ using Student's t-test. **d** Statistics showing the correlation between medium flow speed and stirring bar rotation speed ($R^2 = 0.9373$) **e** Representative photograph of the layout of the dynamic perfusion tissue culture device. **f** Computational simulation of medium flow speed pattern surrounding the tissue. The flow speed on the sheet's front side (recording point is marked by a blue dot) and the back side (recording point is marked by a red dot) is 6.47 cm/s and 2.87 cm/s, respectively. **g** Computational simulation of shear stress caused by fluid flow. The shear stress on the sheet's front side (recording point is marked by a blue dot) and the back side (recording point is marked by a red dot) is 0.18 Pa and 0.013 Pa, respectively

for 30 min. AlexaFlour 647 conjugated isolectin B4 (1:100; Invitrogen) staining was performed following the manufacturer's instructions to evaluate the capillary density in the MI border zone. Images were captured using a confocal microscope (NIKON A1; Nikon) or BIOREVO fluorescence microscope (KEYENCE Corporation) and analyzed using ImageJ.

TUNEL Staining

Frozen sections were used for TUNEL staining using the Click-IT TUNEL kit (C10617 Invitrogen; Thermo Fisher Scientific, Waltham, MA, USA) following the manufacturer's instructions. Images were captured using the BIOREVO fluorescence microscope (KEYENCE Corporation). The percentage of apoptotic nuclei was

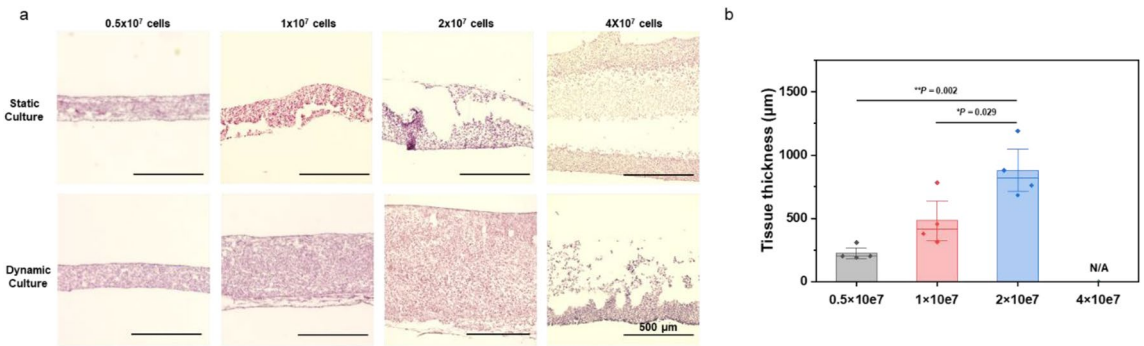

Fig. 2 Cardiac tissue sheets formed on single-layer (0.5×10^7 cells) or multilayer fiber (1, 2, 4×10^7 cells) sheets. **a** Histology of cardiac tissue with different cell seeding densities. **b** Thickness of cardiac tissue with varying cell densities under dynamic culture conditions. Data are represented as means ± SEM, n = 4 independent biological replicates. *$P < 0.05$, **$P < 0.01$ using one-way ANOVA followed by Tukey's post hoc test

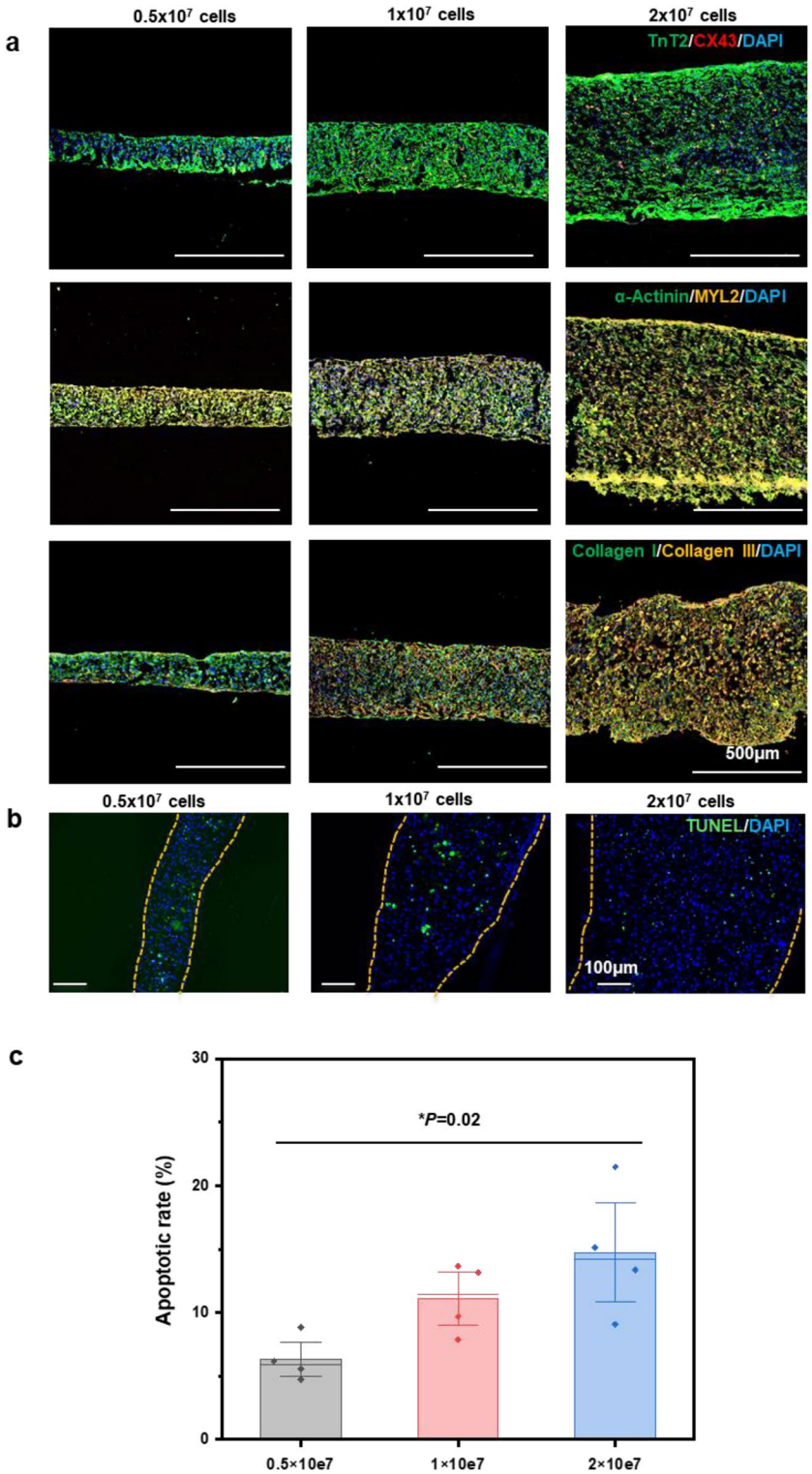

Fig. 3 Representative immunostaining of cardiac tissue sheets under dynamic culture conditions. **a** Staining image of TnT2 (green), CX43 (red), α-Actinin (green), MYL2 (red), Collagen I (green), Collagen III (red), and Fibronectin (red). **b–c** TUNEL staining images and apoptotic rate of cardiac tissue sheets. Data are represented as means ± SEM, n = 4 independent biological replicates. $^{*}P < 0.05$ using one-way ANOVA followed by Tukey's post hoc test

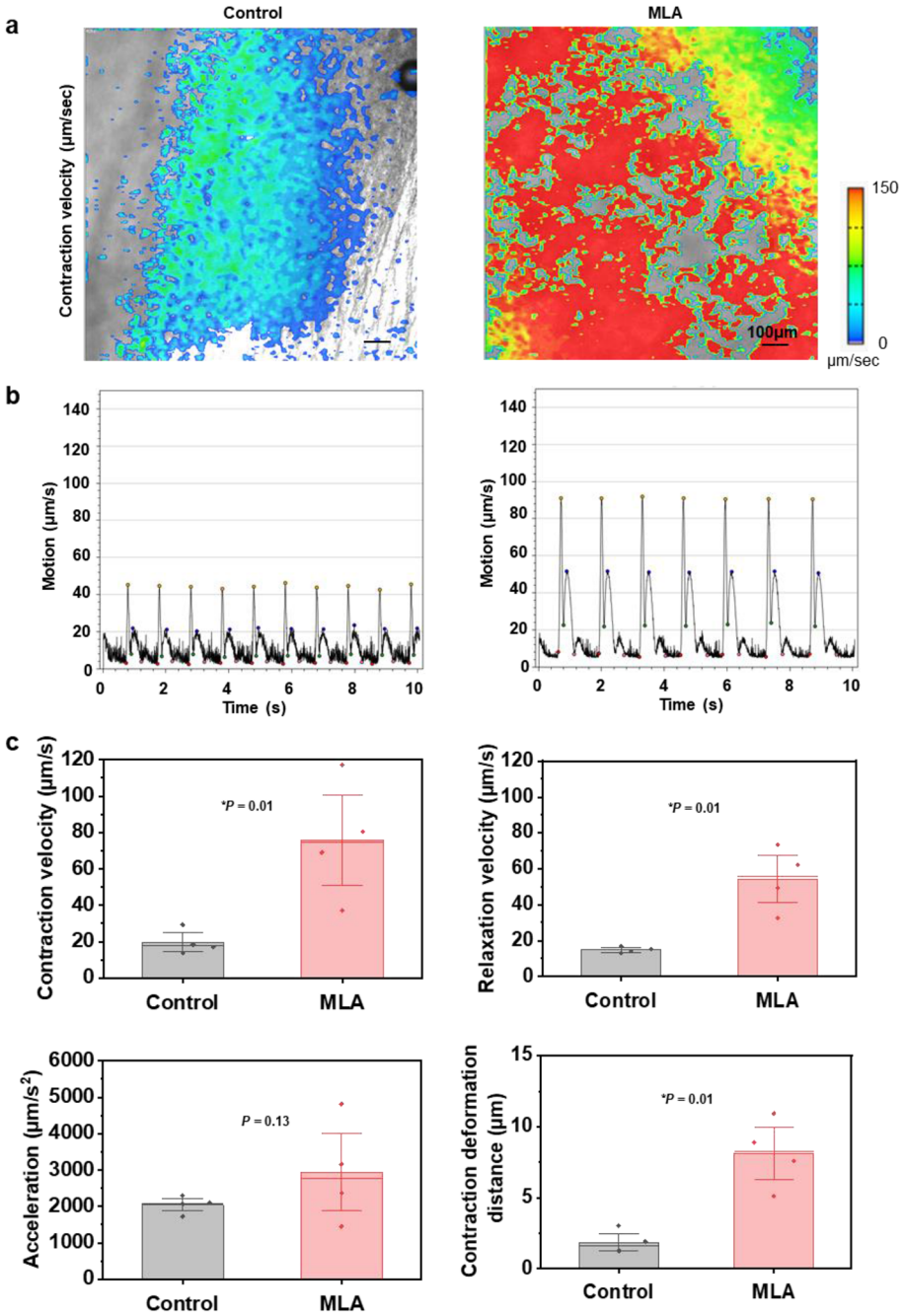

Fig. 4 Motion analysis of multilayer cardiac tissue sheets. **a** Representative velocity image of the cardiac tissue on single-layer fiber sheet (Control: 5×10^6 cells) and multilayer fiber sheets (MLA: 2×10^7 cells) using a motion analysis system. Red and blue color represent high and low velocities, respectively. **b** Plot of a motion waveform showing contraction and relaxation velocity peaks. **c** Contractile properties of the aligned and non-aligned cardiac tissue. Data are represented as means ± SEM, n = 4 independent biological replicates. $^*P<0.05$ using Student's *t*-test

calculated by dividing the total number of TUNEL-stained nuclei by the total number of DAPI-positive nuclei.

ELISA

Culture supernatants of the MLA and control samples were collected and extracted after five days of culture. The concentrations of vascular endothelial growth factor (VEGF), hepatocyte growth factor (HGF), stromal cell-derived factor (SDF-1), interleukin 6 (IL-6), and platelet-derived growth factor subunit B (PDGF-ββ) were measured using an ELISA kit (R&D Systems, Minneapolis, MN, USA) following the manufacturer's instructions. The absorbance rate was determined using a microplate reader (Powerscan

H1, DS Pharma Biomedical, Osaka, Japan) at 450 nm, with a 540 nm wavelength correction.

Electrophysiological Recording Using MEA

The field potentials of the cardiac tissue were recorded using a microelectrode arrays (MEA) data system (USB-ME64-System, Multi-Channel Systems, Germany) with an MC_Rack (Multi-Channel Systems). The activation map was generated using the local activation time from the single electrodes obtained by calculating the minimum of the raw curve's first-derivative plot. Linear interpolation between the electrodes was used to calculate the isochronal map [12, 35] using MATLAB (MATLAB, MathWorks, USA).

Motion Analysis

The contractile properties were evaluated using a cell motion imaging system (SI8000; SONY, Tokyo, Japan). The tissues were cultured for five days. Videos were recorded at a rate of 150 frames per second, a resolution of 1024×1024 pixels, and a depth of 8 bits. For the drug assay, the drugs were mixed into the medium at a certain concentration and prewarmed at 37 °C. After the baseline data were collected, the drug medium was used to replace the old medium. The motion data were again collected 5 min after the medium change. The same groups of MLA samples were first used for the isoproterenol test and then washed with a blank medium before being used for the acetylcholine test.

Statistical Analysis

All quantitative data are presented as mean ± standard error of the mean (SEM). The difference between the two groups was analyzed using a one-tailed Student's *t*-test. Comparisons among multiple groups were analyzed using one-way analysis of variance (ANOVA) followed by Tukey's post hoc test, and statistical significance was set at a $P < 0.05$.

Results

Fabrication of Multilayer Fiber Scaffold for Thick Tissue Culture

In our previous report, a 160-μm-thick cardiac tissue was obtained by seeding CMs on a single-layer fiber sheet [12]. Simply improving the cell number could not further enhance the tissue thickness, potentially resulting in peeling off the tissue from the fiber sheet. In this study, we prepared single-layer fibers via electrospinning as a control. In contrast, a thicker multilayer fiber (MLA) sheet with a three-dimensional structure was fabricated by adding another four top-layer fiber sheets above the bottom-layer fiber sheet, with a space of 150 μm between each of the two layers (Fig. 1a, b). The top-layer fiber sheets were made with lower density and higher porosity (69.52% ± 2.61% vs. 30.61% ± 0.76%, $P < 0.001$) than the bottom-layer fiber (Fig. 1c). The high porosity would facilitate the penetration of cells into the multilayer fiber sheet. Furthermore, stirring bars generated the dynamic

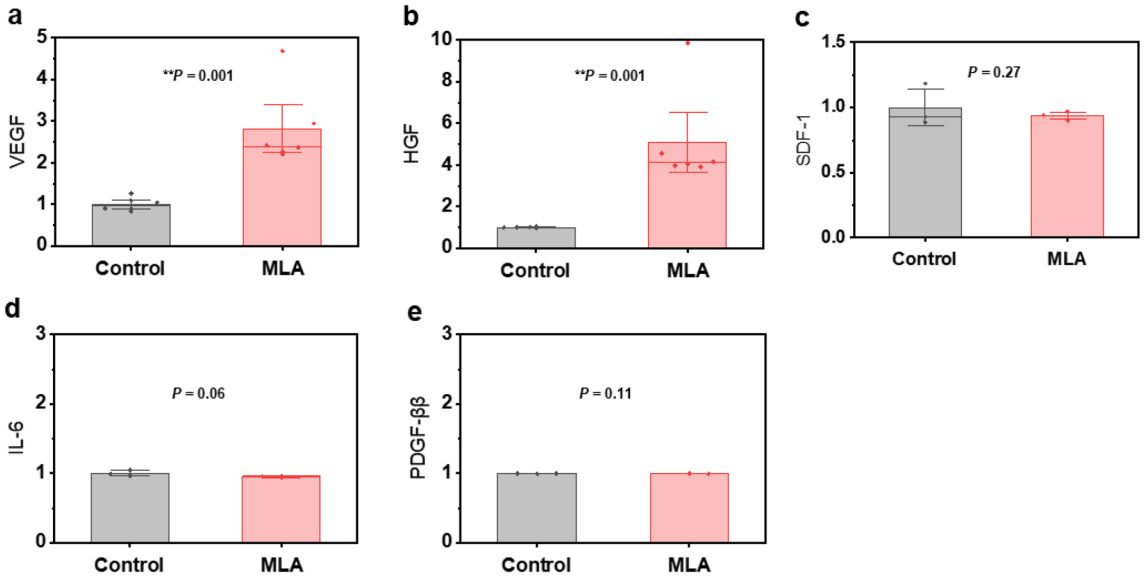

Fig. 5 Normalized cytokine secretion of multilayer cardiac tissue sheets. **a–e** Data are represented as means ± SEM; VEGF, HGF: n = 6, SDF-1, IL-6, PDGF-ββ: n = 3 independent biological replicates. $^{**}P < 0.01$ using Student's *t*-test

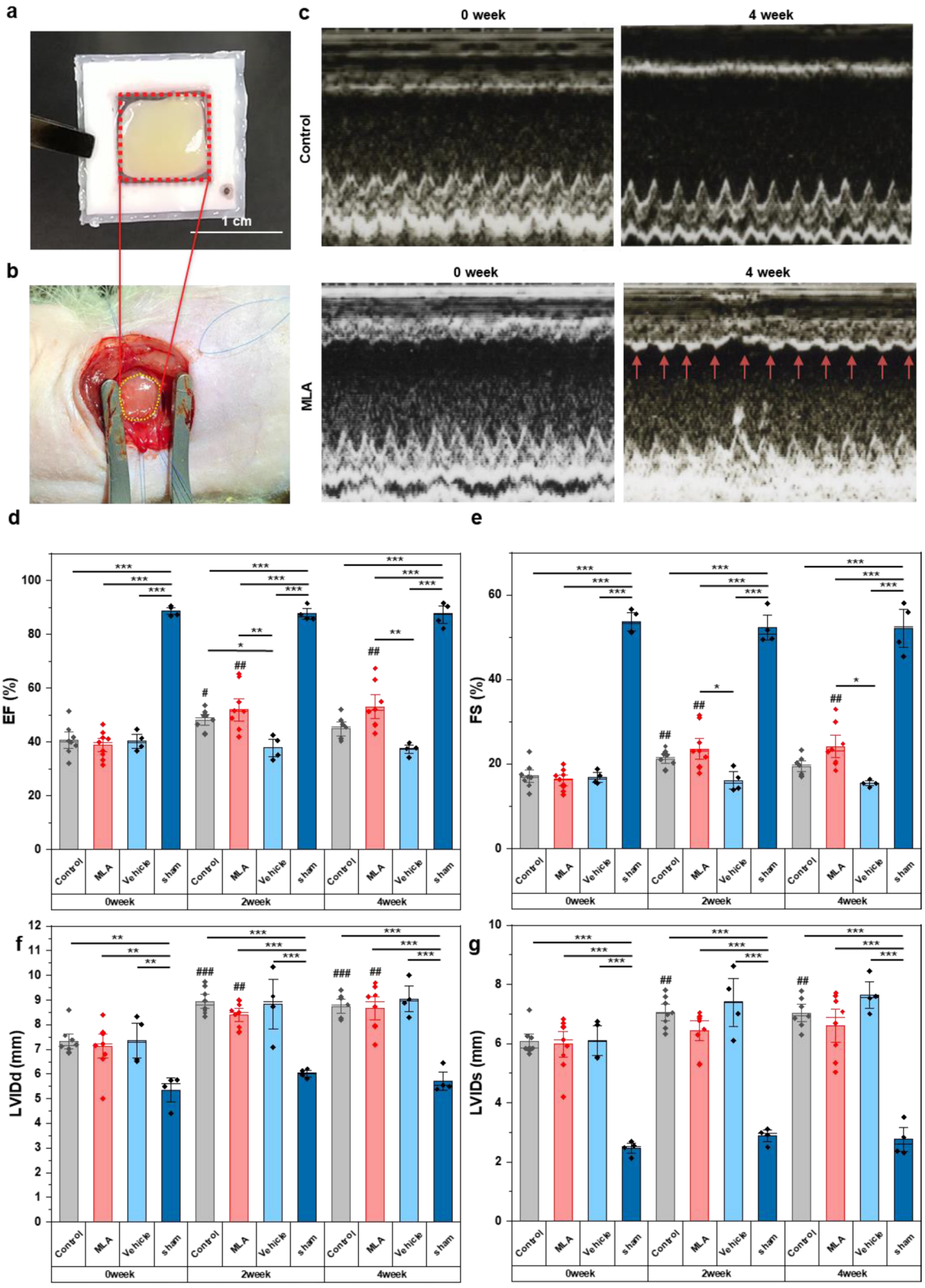
a
1 cm
b
c
0 week
4 week
Control
MLA
d
e
EF (%)
FS (%)
f
g
LVIDd (mm)
LVIDs (mm)
Control
MLA
Vehicle
sham
0week
2week
4week

◂**Fig. 6** Multilayer cardiac tissue sheets transplantation improves cardiac function. **a–b** Representative images of MLA tissue and its transplantation on a rat heart with myocardial infarction. **c** Representative M-mode echocardiography photo of control and MLA groups. **d–g** Change of ejection fraction (EF, d), fractional shortening (FS, e), left ventricular internal dimension at end-diastole (LVIDd, f), and left ventricular internal dimension at end-systole (LVIDs, g) of infarct rat heart following transplantation of MLA, control, vehicle, and sham groups over four weeks. Data are represented as means ± SEM. MLA: n = 9 rats; Control: n = 8 rats; Vehicle: n = 4 rats; Sham: n = 4 rats. $^{*}P < 0.05$, $^{**}P < 0.01$, and $^{***}P < 0.001$ compared two of MLA, control, vehicle, and sham groups using one-way ANOVA followed by Tukey's post hoc test. $^{\#}P < 0.05$ and $^{\#\#}P < 0.01$ compared between 0, 2 and 4 weeks data using one-way ANOVA followed by Tukey's post hoc test

flow for spin culture to promote oxygen and nutrient diffusion in the thick tissue (Fig. 1d, e). The thick tissue was mounted on a holder at a 30° oblique leaning angle to reduce the shear stress caused by the medium flow (Fig. 1e). According to previous reports, shear stress > 1 Pa may lead to cell damage or even death [36, 37]. Additionally, the flow rate of approximately 2 cm/s has proven ideal for three-dimensional tissue culture [31] and is within the range of physiological flow rates in the human body [38]. The flow and shear stress fields under different stirring speeds were simulated and analyzed to evaluate the shear stress in the present design (Fig. 1e, f, S2). Among the multiple conditions simulated, when the flow speed is set to 3.65 cm/s (250 rpm), the flow speed in the back side of the sheet (cell culture area) was lower (as marked by the red point, 2.87 cm/s) than the front side (as marked by blue point, 6.47 cm/s). Similarly, the shear stress on the back side of the sheet was also lesser (0.013 Pa) than that on the front side (0.18 Pa) (Fig. 1f, g). At the flow rate of 3.65 cm/s, the cells seeded on the back side would be able to receive nutrients from the dynamic flow while the shear stress is kept at a safe level, much lower than 1 Pa.

Optimization of the Culture Conditions for Multilayer Tissue

To find the optimal conditions for the construction of cardiac tissue, first, we seeded different numbers of hiPSC-CMs (purity: 90.9% ± 3.04%, Fig. S3) on a single (0.5×10^7 cells) and multilayer fiber sheet (1, 2, and 4×10^7), and evaluated the impact of static and dynamic cultures on the tissue. HE staining data indicated that the dynamic culture improved tissue organization with few hollow areas, especially in thicker tissues (Fig. 2a). Compared with static culture groups, the dynamic culture allowed well-organized tissue formation with thickness ranging from 226.51 ± 28.06 µm to 878.64 ± 111.69 µm (Fig. 2b). However, the tissue with 4×10^7 cells showed dramatically reduced viability, which may be because of limited oxygen and nutrient diffusion within the thick tissue. Additionally, the number of unattached floating cells was higher in the suspension of the laminin- (without laminin) group than those in the laminin+ (with laminin) group. This may indicate that the laminin supplemented into the medium during cell seeding was vital for cell attachment and tissue formation. Electrophysiological data recorded using MEA indicated less homogeneous propagation and smaller electrical signal amplitude in the laminin- group (Fig. S4). Immunostaining revealed a well-defined organization of CMs within the tissue (Fig. 3a),

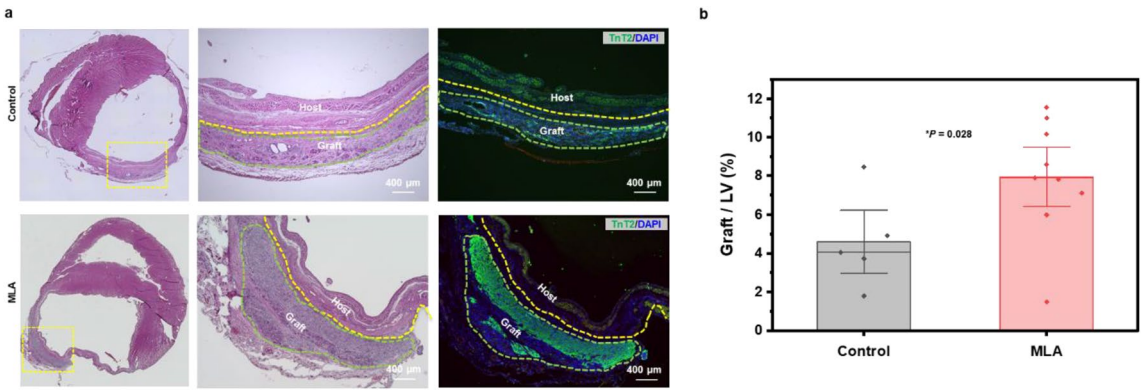

Fig. 7 Engraftment of cardiac tissue sheets four weeks after transplantation. **a** The left panels are histological sections of the control and MLA group after transplantation on the rat heart with myocardial infarction. The right panels show double immunostaining for hTnT (green), and nuclei were stained with DAPI (blue). **b** Statistics showing the TnT2-positive graft/left ventricular ratio of remaining tissue in both groups. Data are represented as means ± SEM. MLA: $n = 9$ rats; Control, $n = 5$ rats. $^{*}P < 0.05$ using Student's t test

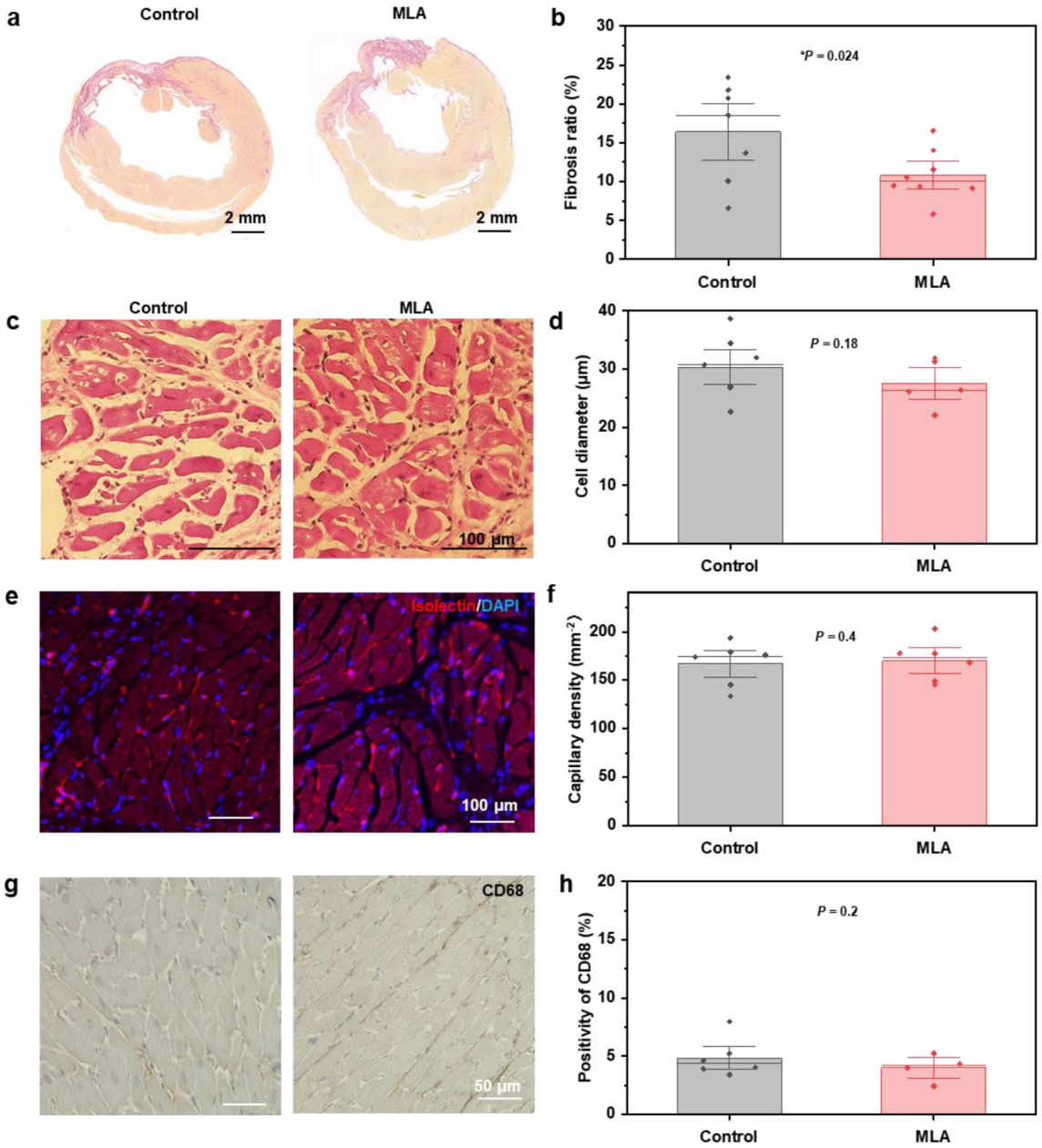

Fig. 8 Histology of the extracted heart four weeks after transplantation. **a–b** Sirius red staining demonstrating fibrosis in both groups. MLA: n = 4 rats; Control. n = 6 rats. **(c–d)** Cell diameter in border zone from both groups. MLA: n = 5 rats; Control. n = 7 rats. **e–f** Counterstaining using Isolectin B4 (red) and DAPI image showing capillaries in the border zone. $n = 6$ rats. **g–h** The CD68 positive cell density in the border zone. MLA: $n = 4$ rats; Control: $n = 6$ rats. Data are represented as means ± SEM. $^*P < 0.05$ using Student's *t*-test

including the well-positioned TnT2 myofilaments and α-actinin-positive sarcomeres. Abundant expression of extracellular matrix proteins (collagen) was also found in the thick tissue. Furthermore, TUNEL staining was used to evaluate the viability of cells within the tissues (Fig. 3b, c). The apoptotic rate of the 2×10^7 group (14.76% ± 2.58%) showed no significant difference from the 1×10^7 group (11.1% ± 1.39%) and was higher than that of 0.5×10^7 group (6.32% ± 0.89%). These results indicated that well-organized, viable,

and thick cardiac tissue could be obtained by culturing CMs on a multilayer fiber sheet.

Comparison of Multilayer and Single-layer Tissue with Motion Analysis and Cytokine Secretion Assay

According to the above results, the 2×10^7 group was the thickest and had the well viability; thus, we compared this group (multilayer group: MLA) with the 5×10^6 group (Control group), which shares the same cell concentration as our previous report [12] for further in vitro and in vivo evaluations. The cardiac tissue contractility was evaluated using a cell motion imaging system (Fig. 4). The MLA group demonstrated significantly higher contraction velocity (75.91 ± 16.46 vs. 19.70 ± 3.36 μm/s, $P = 0.008$), relaxation velocity (54.39 ± 8.73 vs. 14.74 ± 0.8 μm/s, $P = 0.002$) and contraction deformation distance (8.14 ± 1.22 vs. 1.86 ± 0.42 μm; $P = 0.001$), indicating their improved contractile properties. In addition, the MLA tissue could respond to the positive modulation of a β-agonist (isoproterenol) and negative modulation of a neurotransmitter (acetylcholine) (Fig. S5). A previous report has indicated that cytokines secreted by the hiPSC-CM patch could enhance electrical conduction and improve heart function [39]; therefore, we compared the secreted cytokines in the culture supernatants of the two groups (Fig. 5). The MLA group showed significantly higher secretion of angiogenesis-related factors, including VEGF and HGF. No significant differences were found in the secretion of SDF-1, IL-6, and PDGF-ββ between the two groups.

Transplantation of Cardiac Tissue Improved Heart Function of Rat with MI

MLA and control cardiac tissues were transplanted into rats with MI (Fig. 6a, b). Cardiac function was evaluated using echocardiography. Echocardiography indicated that the MLA group showed a significant improvement (Fig. 6c) in the LV ejection fraction after transplantation (0 vs. 4 weeks: $38.8 \pm 1.67\%$ vs. $53.1 \pm 3.0\%$, $P = 0.00163$), whereas the control and vehicle group showed no significant improvement (0 vs. 4 weeks). The ejection fractions (Fig. 6d) were significantly different between the MLA and vehicle groups at 2 ($P = 0.0036$) and 4 weeks ($P = 0.0022$). However, no significant difference exists between the control and vehicle groups at 4 weeks ($P = 0.22$). The MLA group showed significant improvement in fractional shortening (Fig. 6e 0 vs. 4 weeks: $16.2 \pm 0.8\%$ vs. $24.2 \pm 1.8\%$, $P = 0.0022$), whereas both control and vehicle groups showed no significant improvement (0 vs. 4 weeks). Both control and MLA groups showed increased LV dimension at end-diastole in 4 weeks (Fig. 6f). However, the LV end-systolic measurements of the MLA group showed no significant change in 4 weeks (Fig. 6g 0 vs. 4 weeks: 0.598 ± 0.028 cm vs. 0.66 ± 0.037 cm, $P = 0.32$), compared with the increase in the control group (0 vs. 4 weeks: 0.607 ± 0.017 cm vs. 0.704 ± 0.02 cm, $P = 0.0037$). The heart rate variability was also evaluated, and no significant differences were found between the two groups (Fig. S6). These results indicated that the MLA group had improved functional recovery compared with the control and vehicle groups.

Transplantation of MLA Promoted Graft Engraftment of hiPSC-CM and Inhibited Fibrosis in the Host

Transplanted tissue engraftment was evaluated using HE and immunofluorescent staining (Fig. 7) to confirm the survival of transplanted hiPSC-CMs. The MLA group demonstrated retention of a large area of TnT2-positive hiPSC-CM tissue compared with the significantly lower retention in the control group, also evidenced by a significantly higher graft/LV ratio than the control group (MLA vs. Control: 8.0% ± 1% vs. 4.6% ± 1.1%, $P = 0.028$). In addition, the MLA group demonstrated significantly lesser fibrosis in the border zone than the control group (Fig. 8a, b, MLA vs. Control: 10.8% ± 1.2% vs. 16.4% ± 2.4%, $P = 0.024$). No significant differences between the two groups were observed in the cell diameter and capillary density in the border zone (Fig. 8c–f.). CD68 staining revealed no significant inflammatory reactions in both groups at 4 weeks after transplantation (Fig. 8g, h, MLA vs. Control: 4.0% ± 0.59% vs. 4.86% ± 0.67%, $P = 0.198$). These results indicated that a higher dose of hiPSC-CMs in the MLA group could enhance functional recovery and lower fibrosis in the infarcted heart.

Discussion

Transplanting thick and viable cardiac tissue to treat MI is challenging. Cell sheets were stacked to achieve thick cardiac tissue. Sakaguchi et al. developed bioreactors that can perfuse thick tissues. They sequentially overlapped 12 sheets over several days and obtained a 100-μm thick cardiac [40]. Recently, Matsuo et al. developed a simplified method to stack 15 cell sheets with the insertion of gelatin hydrogel microspheres for promoting oxygen diffusion [26]. The overlaying process takes several hours, and the resulting cardiac sheet is approximately 1 mm thick (0.67 mm for cellular components). Our group has also tried to overlay seven cell sheets (100 μm) under the omentum covering during transplantation, which enhanced the survival of hiPSC-CMs [14]. Increasing the number of cell sheet layers is straightforward and demonstrates

the therapeutic advantage of thick tissues. However, these methods require the preparation of single-cell sheets and subsequent overlaying, which requires considerable effort before and during transplantation.

Alternatively, our group developed cardiac tissue-like constructs by seeding hiPSC-CMs on a low-thickness, aligned, fibrous scaffold made of biodegradable poly (D,L-lactic-co-glycolic acid) polymer. The multilayered aligned CMs could be organized at a high-density along the aligned nanofibers in a simple one-step seeding process, resulting in upregulated cardiac biomarkers and enhanced cardiac functions [12]. We validated the therapeutic effect of the fibrous scaffold-based tissue sheet on a rat and human-relevant porcine ischemic cardiomyopathy model, respectively [12, 30]. The fibrous scaffold area can easily be increased to obtain a larger tissue sheet; however, the thickness cannot be increased simply by increasing the seeded cell number because this could lead to the peeling off of the tissue from the fibrous scaffold. In the present study, we further developed an integrated multilayer fibrous scaffold composed of one layer of thick and several layers of thin fibers. The integrated multilayer structure allowed the penetration of cells in the one-step seeding process and prevented the detachment of the thick tissue (878.64 ± 193.45 µm) from the fibrous scaffold. The thick cardiac tissue showed improved contraction and higher cytokine secretion than the thin one. When used to treat a rat MI model, the multilayer group demonstrated improved functional recovery, reduced fibrosis, and no significant signs of inflammatory reaction. The multilayer group showed improved VEGF secretion (Fig. 5); however, no significant difference in capillary density (angiogenesis) was observed between the two groups (Fig. 8e, f). In addition, TnT2-positive cell retention in the MLA group was significantly higher than in the control group (Fig. 7). This may indicate that the enhanced therapeutic effect of the MLA group may be related to remuscularization rather than the cytokine effect.

The maximum cell number that the present multilayer scaffold could hold was 2×10^7 for a 1-cm^2 culture area, similar to a recently published report on the correlation between ventricular function improvement and the dose of hiPSC-CM [6]. Considering that the size of the present scaffold (rat heart) was 1×1 cm^2, the scaffold for the human heart will be significantly larger (~50 cm^2), and engrafted CM number would be increased to 1×10^9, which will be approximately 1/3 of the CM number of an adult human heart and sufficient for treating its infarcted part [6]. Of course, there are still some problems to be solved for such a huge number of cells to be used in heart transplantation, such as reducing immune rejection, ensuring cell production and stable supply, and reducing costs.

The present study focused on improving the thickness of engineered cardiac tissue, and most cells within the multilayer cardiac tissue were CMs. The human heart is composed of multiple cell types, such as CMs and non-CMs, including cardiac endothelial cells, vascular stromal cells, and cardiac fibroblasts [41]. Our future work will focus on building multilayer cardiac tissues using multiple cell types that mimic in vivo conditions. In particular, we look forward to further realizing nutrient supply by adding vascular endothelial cells. In addition, to achieve better therapeutic effects, the maturation of hiPSC-CMs must be further improved to the adult level, including enhanced contractile properties, metabolism, and cellular structure.

Aside from cardiac tissue, biodegradable multilayer fiber scaffolds may also be used to prepare other types of tissues, such as skin, corneal, oral mucosal epithelial, cartilage, and fibroblast tissues. This one-step preparation and easy-to-handle features may facilitate future clinical applications. Artificial meat has been under intensified investigation as a potential human food source [42]. Because of the similarity between cardiac and skeletal muscle tissues, multilayer fibers may also be used for making artificial skeletal tissue as artificial meat.

In conclusion, we developed a multilayer fibrous scaffold to create one-step thick and viable cardiac tissue sheets. The multilayer tissue showed improved contraction and cytokine secretion, whereas cell viability was maintained in vitro. In the rat MI model, the multilayer group demonstrated improved functional recovery and less fibrosis than the single-layer group, indicating that appropriate hiPSC-CM dose requires careful evaluation for clinical therapy development.

Supplementary Information The online version contains supplementary material available at https://doi.org/10.1007/s42765-023-00313-4.

Author Contributions JL, YS, SM, and LL conceived the project. JL, XQ, TK, RM, YS, SM, and LL designed the experiments. JL, XQ, LLJ, YH, J.Z, KS, MI, NY, AT, NS, EI and AH, performed the experiments. JL, YS, SM and LL contributed to funding acquisition. All authors contributed to data analysis and interpretation. JL, XQ, LL and SM drafted the manuscript.

Funding Open access funding provided by Osaka University. This research was supportedby the Japan Agency for Medical Research and Development (AMED) under GrantNumber jp22bm0204003h, the Japan Society for the Promotion of Science (JSPS)Grant-in-Aid for Scientific Research (A) under Grant Number 20H00542, and Grant-in-Aidfor Scientific Research (B) under Grant Number (22H03157). X. Qu was supportedby the Ministry of Education, Culture, Sports, Science, and Technology (MEXT)scholarship.

Data availability The data are available from the corresponding author on reasonable request.

Declarations

Conflict of interest The authors declare no competing non-financial interests but the following competing financial interests. Y.S.'s laboratory received funding from the Cuorips Company.

References

1. Li J, Liu L, Zhang J, Qu X, Kawamura T, Miyagawa S, Sawa Y. Engineered tissue for cardiac regeneration: current status and future perspectives. Bioengineering (Basel). **2022**;*9*:605.
2. Kobayashi H, Tohyama S, Kanazawa H, Ichimura H, Chino S, Tanaka Y, Suzuki Y, Zhao J, Shiba N, Kadota S, Narita K, Naito T, Seto T, Kuwahara K, Shiba Y, Fukuda K. Intracoronary transplantation of pluripotent stem cell-derived cardiomyocytes: Inefficient procedure for cardiac regeneration. J Mol Cell Cardiol. **2023**;*174*:77.
3. Funakoshi S, Fernandes I, Mastikhina O, Wilkinson D, Tran T, Dhahri W, Mazine A, Yang D, Burnett B, Lee J, Protze S, Bader GD, Nunes SS, Laflamme M, Keller G. Generation of mature compact ventricular cardiomyocytes from human pluripotent stem cells. Nat Commun. **2021**;*12*:3155.
4. Nakazato T, Kawamura T, Uemura T, Liu L, Li J, Sasai M, Harada A, Ito E, Iseoka H, Toda K, Sawa Y, Miyagawa S. Engineered three-dimensional cardiac tissues maturing in a rotating wall vessel bioreactor remodel diseased hearts in rats with myocardial infarction. Stem Cell Reports. **2022**;*17*:1170.
5. Huang K, Ozpinar EW, Su T, Tang J, Shen D, Qiao L, Hu S, Li Z, Liang H, Mathews K, Scharf V, Freytes DO, Cheng K. An off-the-shelf artificial cardiac patch improves cardiac repair after myocardial infarction in rats and pigs. Sci Transl Med. **2020**;*12*:eaat9683.
6. Querdel E, Reinsch M, Castro L, Kose D, Bahr A, Reich S, Geertz B, Ulmer B, Schulze M, Lemoine MD, Krause T, Lemme M, Sani J, Shibamiya A, Studemann T, Kohne M, Bibra CV, Hornaschewitz N, Pecha S, Nejahsie Y, Mannhardt I, Christ T, Reichenspurner H, Hansen A, Klymiuk N, Krane M, Kupatt C, Eschenhagen T, Weinberger F. Human Engineered Heart tissue patches remuscularize the injured heart in a dose-dependent manner. Circulation. **2021**;*143*:1991.
7. Tabei R, Kawaguchi S, Kanazawa H, Tohyama S, Hirano A, Handa N, Hishikawa S, Teratani T, Kunita S, Fukuda J, Mugishima Y, Suzuki T, Nakajima K, Seki T, Kishino Y, Okada M, Yamazaki M, Okamoto K, Shimizu H, Kobayashi E, Tabata Y, Fujita J, Fukuda K. Development of a transplant injection device for optimal distribution and retention of human induced pluripotent stem cell–derived cardiomyocytes. J Heart Lung Transplant. **2019**;*38*:203.
8. Shiba Y, Fernandes S, Zhu WZ, Filice D, Muskheli V, Kim J, Palpant NJ, Gantz J, Moyes KW, Reinecke H, Van Biber B, Dardas T, Mignone JL, Izawa A, Hanna R, Viswanathan M, Gold JD, Kotlikoff MI, Sarvazyan N, Kay MW, Murry CE, Laflamme MA. Human ES-cell-derived cardiomyocytes electrically couple and suppress arrhythmias in injured hearts. Nature. **2012**;*489*:322.
9. Shiba Y, Gomibuchi T, Seto T, Wada Y, Ichimura H, Tanaka Y, Ogasawara T, Okada K, Shiba N, Sakamoto K, Ido D, Shiina T, Ohkura M, Nakai J, Uno N, Kazuki Y, Oshimura M, Minami I, Ikeda U. Allogeneic transplantation of iPS cell-derived cardiomyocytes regenerates primate hearts. Nature. **2016**;*538*:388.
10. Liao S-Y, Liu Y, Siu C-W, Zhang Y, Lai W-H, Au K-W, Lee Y-K, Chan Y-C, Yip PM-C, Wu EX. Proarrhythmic risk of embryonic stem cell–derived cardiomyocyte transplantation in infarcted myocardium. Heart Rhythm. **2010**;*7*:1852.
11. Ichimura H, Shiba Y. Recent progress using pluripotent stem cells for cardiac regenerative therapy. Circ J. **2017**;*81*:929.
12. Li J, Minami I, Shiozaki M, Yu L, Yajima S, Miyagawa S, Shiba Y, Morone N, Fukushima S, Yoshioka M, Li S, Qiao J, Li X, Wang L, Kotera H, Nakatsuji N, Sawa Y, Chen Y, Liu L. Human pluripotent stem cell-derived Cardiac tissue-like constructs for repairing the Infarcted myocardium. Stem Cell Reports. **2017**;*9*:1546.
13. Masumoto H, Nakane T, Tinney JP, Yuan F, Ye F, Kowalski WJ, Minakata K, Sakata R, Yamashita JK, Keller BB. The myocardial regenerative potential of three-dimensional engineered cardiac tissues composed of multiple human iPS cell-derived cardiovascular cell lineages. Sci Rep. **2016**;*6*:29933.
14. Kawamura M, Miyagawa S, Fukushima S, Saito A, Miki K, Ito E, Sougawa N, Kawamura T, Daimon T, Shimizu T, Okano T, Toda K, Sawa Y. Enhanced survival of transplanted human induced pluripotent stem cell-derived cardiomyocytes by the combination of cell sheets with the pedicled omental flap technique in a porcine heart. Circulation. **2013**;*128*:87.
15. Guo R, Wan F, Morimatsu M, Xu Q, Feng T, Yang H, Gong Y, Ma S, Chang Y, Zhang S, Jiang Y, Wang H, Chang D, Zhang H, Ling Y, Lan F. Cell sheet formation enhances the therapeutic effects of human umbilical cord mesenchymal stem cells on myocardial infarction as a bioactive material. Bioact Mater. **2021**;*6*:2999.
16. Jiang Y, Sun SJ, Zhen Z, Wei R, Zhang N, Liao SY, Tse HF. Myocardial repair of bioengineered cardiac patches with decellularized placental scaffold and human-induced pluripotent stem cells in a rat model of myocardial infarction. Stem Cell Res Ther. **2021**;*12*:13.
17. Gao L, Gregorich ZR, Zhu W, Mattapally S, Oduk Y, Lou X, Kannappan R, Borovjagin AV, Walcott GP, Pollard AE, Fast VG, Hu X, Lloyd SG, Ge Y, Zhang J. Large cardiac muscle Patches Engineered from Human Induced-Pluripotent Stem Cell-Derived Cardiac cells improve recovery from myocardial infarction in Swine. Circulation. **2018**;*137*:1712.
18. Zhang J, Zhu W, Radisic M, Vunjak-Novakovic G. Can we engineer a human Cardiac Patch for Therapy? Circ Res. **2018**;*123*:244.
19. Miyagawa S, Kainuma S, Kawamura T, Suzuki K, Ito Y, Iseoka H, Ito E, Takeda M, Sasai M, Mochizuki-Oda N, Shimamoto T, Nitta Y, Dohi H, Watabe T, Sakata Y, Toda K, Sawa Y. Case report: transplantation of human induced pluripotent stem cell-derived cardiomyocyte patches for ischemic cardiomyopathy. Front Cardiovasc Med. **2022**;*9*:950829.
20. Miyagawa S, Kawamura T, Ito E, Takeda M, Iseoka H, Yokoyama J, Harada A, Mochizuki-Oda N, Imanishi-Ochi Y, Li J. Evaluation of the efficacy and safety of a clinical grade human induced pluripotent stem cell-derived cardiomyocyte patch a pre-clinical study. BioRxiv. **2021**. https://doi.org/10.1101/2021.04.07.438744.
21. Miyagawa S, Domae K, Yoshikawa Y, Fukushima S, Nakamura T, Saito A, Sakata Y, Hamada S, Toda K, Pak K, Takeuchi M, Sawa Y. Phase I clinical trial of autologous stem cell-sheet transplantation therapy for treating cardiomyopathy. J Am Heart Assoc. *2017*;*6*:e003918.
22. Zhu K, Wu Q, Ni C, Zhang P, Zhong Z, Wu Y, Wang Y, Xu Y, Kong M, Cheng H, Tao Z, Yang Q, Liang H, Jiang Y, Li Q, Zhao J, Huang J, Zhang F, Chen Q, Li Y, Chen J, Zhu W, Yu H, Zhang

J, Yang HT, Hu X, Wang J. Lack of remuscularization following transplantation of human embryonic stem cell-derived cardiovascular progenitor cells in infarcted nonhuman primates. Circ Res. **2018**;*122*:958.
23. Hu X, Xu Y, Zhong Z, Wu Y, Zhao J, Wang Y, Cheng H, Kong M, Zhang F, Chen Q, Sun J, Li Q, Jin J, Li Q, Chen L, Wang C, Zhan H, Fan Y, Yang Q, Yu L, Wu R, Liang J, Zhu J, Wang Y, Jin Y, Lin Y, Yang F, Jia L, Zhu W, Chen J, Yu H, Zhang J, Wang J. A large-scale investigation of hypoxia-preconditioned allogeneic mesenchymal stem cells for myocardial repair in Nonhuman Primates: paracrine activity without remuscularization. Circ Res. **2016**;*118*:970.
24. Liu C-Y, Matsusaki M, Akashi M. Control of cell–cell distance and cell densities in millimeter-sized 3D tissues constructed by collagen nanofiber coating techniques. ACS Biomater Sci Eng. **2015**;*1*:639.
25. Fleischer S, Shapira A, Feiner R, Dvir T. Modular assembly of thick multifunctional cardiac patches. Proc Natl Acad Sci U S A. **2017**;*114*:1898.
26. Matsuo T, Masumoto H, Tajima S, Ikuno T, Katayama S, Minakata K, Ikeda T, Yamamizu K, Tabata Y, Sakata R, Yamashita JK. Efficient long-term survival of cell grafts after myocardial infarction with thick viable cardiac tissue entirely from pluripotent stem cells. Sci Rep. **2015**;*5*:16842.
27. Sekine H, Shimizu T, Sakaguchi K, Dobashi I, Wada M, Yamato M, Kobayashi E, Umezu M, Okano T. In vitro fabrication of functional three-dimensional tissues with perfusable blood vessels. Nat Commun. **2013**;*4*:1399.
28. Liu CY, Matsusaki M, Akashi M. Three-dimensional tissue models constructed by cells with nanometer- or micrometer-sized films on the surfaces. Chem Rec. **2016**;*16*:783.
29. Qu X, Li J, Liu L, Zhang J, Hua Y, Suzuki K, Harada A, Ishida M, Yoshida N, Okuzaki D, Sakai Y, Sawa Y, Miyagawa S. ONO-1301 enhances post-transplantation survival of human induced pluripotent stem cell-derived cardiac tissue sheet by promoting angiogenesis. J Heart Lung Transplant. **2023**;*42*:716.
30. Suzuki K, Miyagawa S, Liu L, Kawamura T, Li J, Qu X, Harada A, Toda K, Yoshioka D, Kainuma S, Kawamura A, Sawa Y. Therapeutic efficacy of large aligned cardiac tissue derived from induced pluripotent stem cell in a porcine ischemic cardiomyopathy model. J Heart Lung Transplant. **2021**;*40*:767.
31. Jackman CP, Carlson AL, Bursac N. Dynamic culture yields engineered myocardium with near-adult functional output. Biomaterials. **2016**;*111*:66.
32. Radisic M, Malda J, Epping E, Geng W, Langer R, Vunjak-Novakovic G. Oxygen gradients correlate with cell density and cell viability in engineered cardiac tissue. Biotechnol Bioeng. **2006**;*93*:332.
33. Yokoyama J, Miyagawa S, Akagi T, Akashi M, Sawa Y. Human induced pluripotent stem cell-derived three-dimensional cardiomyocyte tissues ameliorate the rat ischemic myocardium by remodeling the extracellular matrix and cardiac protein phenotype. PLoS ONE. **2021**;*16*:e0245571.
34. Memon IA, Sawa Y, Fukushima N, Matsumiya G, Miyagawa S, Taketani S, Sakakida SK, Kondoh H, Aleshin AN, Shimizu T, Okano T, Matsuda H. Repair of impaired myocardium by means of implantation of engineered autologous myoblast sheets. J Thorac Cardiovasc Surg. **2005**;*130*:1333.
35. Meiry G, Reisner Y, Feld Y, Goldberg S, Rosen M, Ziv N, Binah O. Evolution of action potential propagation and repolarization in cultured neonatal rat ventricular myocytes. J Cardiovasc Electrophysiol. **2001**;*12*:1269.
36. Tanzeglock T, Soos M, Stephanopoulos G, Morbidelli M. Induction of mammalian cell death by simple shear and extensional flows. Biotechnol Bioeng. **2009**;*104*:360.
37. Mardikar SH, Niranjan K. Observations on the shear damage to different animal cells in a concentric cylinder viscometer. Biotechnol Bioeng. **2000**;*68*:697.
38. Björnmalm M, Faria M, Chen X, Cui J, Caruso F. Dynamic flow impacts cell–particle interactions: sedimentation and particle shape effects. Langmuir. **2016**;*32*:10995.
39. Lancaster JJ, Sanchez P, Repetti GG, Juneman E, Pandey AC, Chinyere IR, Moukabary T, LaHood N, Daugherty SL, Goldman S. Human induced pluripotent stem cell–derived cardiomyocyte patch in rats with heart failure. Ann Thorac Surg. **2019**;*108*:1169.
40. Sakaguchi K, Shimizu T, Horaguchi S, Sekine H, Yamato M, Umezu M, Okano T. In vitro engineering of vascularized tissue surrogates. Sci Rep. **2013**;*3*:1316.
41. Giacomelli E, Meraviglia V, Campostrini G, Cochrane A, Cao X, van Helden RWJ, Krotenberg Garcia A, Mircea M, Kostidis S, Davis RP, van Meer BJ, Jost CR, Koster AJ, Mei H, Miguez DG, Mulder AA, Ledesma-Terron M, Pompilio G, Sala L, Salvatori DCF, Slieker RC, Sommariva E, de Vries AAF, Giera M, Semrau S, Tertoolen LGJ, Orlova VV, Bellin M, Mummery CL. Human-iPSC-derived cardiac stromal cells enhance maturation in 3D cardiac microtissues and reveal non-cardiomyocyte contributions to heart disease. Cell Stem Cell. **2020**;*26*:862.
42. Kang DH, Louis F, Liu H, Shimoda H, Nishiyama Y, Nozawa H, Kakitani M, Takagi D, Kasa D, Nagamori E, Irie S, Kitano S, Matsusaki M. Engineered whole cut meat-like tissue by the assembly of cell fibers using tendon-gel integrated bioprinting. Nat Commun. **2021**;*12*:5059.